




Domain wall damped harmonic oscillations induced by curvature gradients in elliptical magnetic nanowires

G. H. R. Bittencourt ^{1,*}, S. Castillo-Sepúlveda,² O. Chubykalo-Fesenko,³ R. Moreno ⁴,
D. Altbir ⁵ and V. L. Carvalho-Santos¹

¹*Departamento de Física, Universidade Federal de Viçosa, 36570-900, Viçosa, Brazil*

²*Grupo de investigación en Física Aplicada, Facultad de Ingeniería, Universidad Autónoma de Chile, Avda. Pedro de Valdivia 425, Providencia, Chile*

³*Instituto de Ciencia de Materiales de Madrid, CSIC, Cantoblanco, 28049 Madrid, Spain*

⁴*Earth and Planetary Science, School of Geosciences, University of Edinburgh, Edinburgh EH9 3FE, United Kingdom*

⁵*Universidad de Santiago de Chile, Departamento de Física, CEDENNA, 9170124, Santiago, Chile*



(Received 11 July 2022; revised 14 September 2022; accepted 8 November 2022; published 21 November 2022)

This paper focuses on the dynamics of a domain wall (DW) displacing along an elliptically bent nanowire (NW) under the action of spin-polarized electric currents and external magnetic fields. Our results evidence that a curvature gradient induces an exchange-driven effective tangential field responsible for pinning a DW at the maximum curvature point in the NW. However, the competition between the torques produced by the external stimuli and the curvature-induced effective fields changes the DW equilibrium position and phase. Therefore, when the external stimuli are below a certain threshold, the DW follows a damped harmonic oscillation around the new equilibrium position. Above this threshold, DW displaces along the NW under an oscillatory translational motion.

DOI: [10.1103/PhysRevB.106.174424](https://doi.org/10.1103/PhysRevB.106.174424)

I. INTRODUCTION

Magnetic nanowires (NWs) are promising candidates to create a new generation of spin-based devices at the nanoscale. Their geometry-induced strong uniaxial anisotropy parallel to the NW axis [1] allows us to guide domain walls (DWs) along their longer dimension through external magnetic fields and/or electric currents [2–4]. The proper control of the DW dynamics is a key point for developing technologies that use these magnetization textures as information carriers [5,6], nano oscillators [7,8], logic gates [9–11], and nanoantennas [12]. Consequently, controlling the DW dynamical response to external stimuli is a very hot topic in material sciences.

Tuning DW dynamical properties by means of geometrical considerations is a well-established strategy. One example in this direction is the shaping of the NW cross section. In magnetic nanostripes, there exists a threshold for the intensity of the external stimuli known as Walker breakdown [13,14], at which the DW drastically alters its dynamical behavior. Below this limit, the DW propagates constantly and its velocity is linearly proportional to the intensity of the stimuli. Above this limit, the DW exhibits an oscillatory behavior along the stimuli direction and the average velocity losses its linearity. By shaping the NW cross section, the Walker limit can be either suppressed (circular cross section [15]) or engineered, i.e., tuning the amplitude and frequency of the oscillations (polygonal cross sections [16]).

Bending NWs is an alternative strategy to tune DW dynamical properties that has recently attracted lots of attention. In this case, the Walker regime is presented even for NWs with circular cross sections. In bent NWs, the origin of the Walker breakdown is in the curvature-induced exchange torque, while in straight ones the dipolar energy coming from the cross-section shape is the source of this effect. Importantly, in NWs with a constant curvature, the threshold for the Walker breakdown as well as the amplitude of the oscillations can be controlled by means of the curvature [17–19] but not the frequency. Nevertheless, combining both bending and shaping cross sections, e.g., bent nanostripes, can be used to control the frequency of the oscillations. An interesting result is that in bent nanostripes the external stimuli exhibit an extra threshold in which the DW reorients by changing its phase [20].

Introducing a curvature gradient in bent NWs provides extra and intriguing dynamical properties to the DW (or other localized objects such as vortices or skyrmions) motion. In this case, it was shown that their centers of mass displacing along a low-dimensional nanomagnet with a variable mean curvature would suffer the effects of an effective force [21] due to a curvature-induced effective anisotropy and Dzyaloshinskii-Moriya interactions [22,23]. This curvature-induced effective force is responsible, for example, for exciting phenomena such as the attraction and/or repulsion of skyrmions by a curved bump in a nanoshell [21,24,25] and the displacement of transverse DW along a helicoidal NW even in the absence of external fields or electric currents [26]. In particular, Yershov *et al.* [27] analyzed the existence of a pinning potential at the NW maximum curvature region in a torsionless NW with variable curvature. In that paper, the authors studied the DW motion near the maximum curvature

*bittencourt.g.h.r@gmail.com

region, obtaining DW harmonic decaying oscillations [27]. The works cited above evidence that an adequate choice of the NW geometric and magnetic parameters allows the control of the DW position, velocity, and phase.

Motivated by these results, through analytical and numerical calculations within the Thiele approach of a rigid DW, we deeply analyze the dynamics of a DW displacing along an elliptically curved NW under the action of electric currents and magnetic fields. Since this system presents a curvature gradient, the emergence of an effective exchange-driven curvature-induced tangential magnetic field is responsible for pinning the DW near the maximum curvature region of the NW, as also observed by Yershov *et al.* [27]. We also show that the DW equilibrium position depends on the competition between the torques produced by the external stimuli and the exchange-driven curvature-induced tangential effective field. Additionally, we obtain that the DW follows a damped harmonic oscillation if the external stimuli are below a critical threshold. Above this threshold value, the DW propagates following an oscillatory motion along the NW with variable amplitude.

This work is organized as follows: Section II presents the theoretical model adopted in this work. In Sec. III, we present the DW dynamics in the absence of external stimuli while Secs. IV and V describe the DW dynamics under an external current or magnetic field, respectively. Our conclusions are presented in Sec. VI.

II. THEORETICAL MODEL

A. General formulation

The geometrical description of an arbitrary curvilinear NW without torsion can be done by adopting an orthogonal basis $(\hat{\mu}, \hat{\eta}, \hat{z})$, where $\hat{\eta}$ is an azimuthal-like direction, which points tangent to the NW axis, and $\hat{\mu}$ is a radial-like unitary vector pointing outward from the bend, perpendicular to the NW axis [see Fig. 1(a)]. The third unitary vector of the considered basis points along the z -axis direction, and can be defined from $\hat{z} = \hat{\mu} \times \hat{\eta}$ and therefore, vectors $\hat{\mu}$ and $\hat{\eta}$ lie in the xy Cartesian plane. Under this framework, a NW can be described as $\mathbf{r}(\mu, \eta, z) = (x, y, z)$, where $x \equiv x(\mu, \eta)$ and $y \equiv y(\mu, \eta)$. In addition to the unitary vectors, it is important to determine the length element in a curvilinear orthogonal basis along an arbitrary direction $\hat{\xi}$, which is formally defined as $dq_{\xi} = h_{\xi} d\xi$. Here, $h_{\xi} = \sqrt{(\partial \mathbf{r} / \partial \xi) \cdot (\partial \mathbf{r} / \partial \xi)}$ is the modulus of the metric factor associated to the ξ -direction and $\hat{\xi} = h_{\xi}^{-1} \partial \mathbf{r} / \partial \xi$.

This paper considers a thin wire with a circular cross section narrow enough to host a transverse DW when considering a permalloy NW [28]. It is worth noting that other types of DWs could be nucleated in thicker NWs, such as vortex-antivortex and Bloch point walls [28,29]. In our paper, we use the micromagnetism theory to analyze the dynamics of a rigid transverse DW (fixed shape and width) during its displacement along the NW. Therefore, each magnetic moment of the system follows the same dynamics of the DW center. The transverse DW magnetization profile can be written in terms of the arbitrary curvilinear basis as $\mathbf{m} = \sin \Omega \sin \phi \hat{\mu} + \cos \Omega \hat{\eta} + \sin \Omega \cos \phi \hat{z}$, where $\mathbf{m} = \mathbf{M} / M_s$, and M_s is the saturation magnetization. The parameter Ω is the angle between

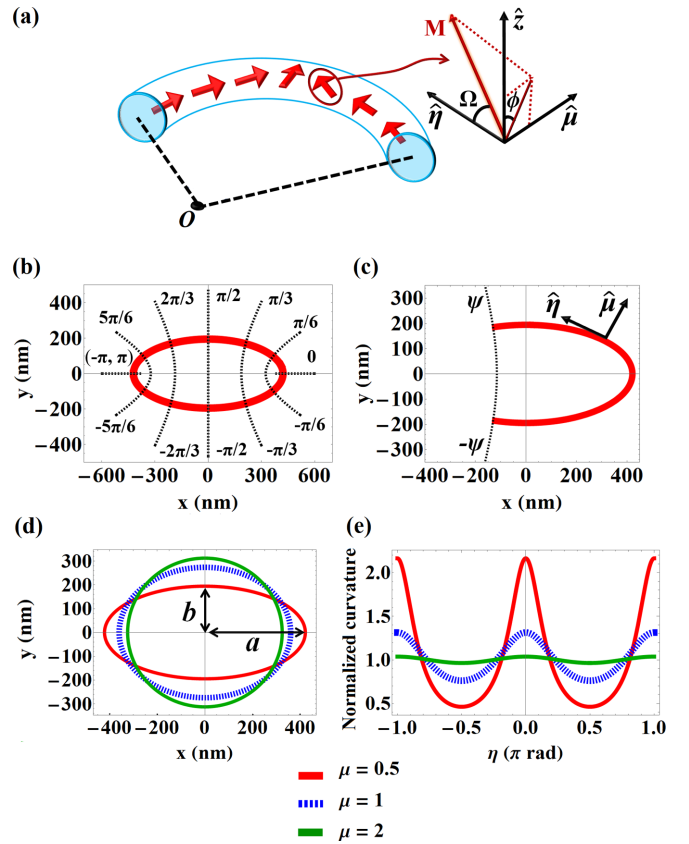


FIG. 1. (a) Representation of the DW magnetization profile lying in an elliptical NW with center located at O (Cartesian origin). (b) Set of hyperbolas (black dashed lines) that intersect orthogonally to the ellipse (red line), defining different values for the η coordinate. (c) Representation of the tangential ($\hat{\eta}$) and normal ($\hat{\mu}$) directions on the elliptical NW delimited by the hyperbola segments defined by $\eta = -\psi$ and $\eta = \psi$. (d) Illustration of three ellipses with perimeter $\mathcal{P} = 2000$ nm and different μ values. (e) Curvature \mathcal{C} of complete ellipses as a function of η for different μ values.

\mathbf{m} and the azimuthal-like unitary vector $\hat{\eta}$, while ϕ is the angle between the magnetization projection in the μz -plane and the vector \hat{z} , as shown in Fig. 1(a). Furthermore, as the dimensions of the NW cross section are much smaller than its length, we can assume that the magnetization distribution varies only along the NW length [$\mathbf{m} = \mathbf{m}(\eta)$], and it is uniform along the $\hat{\mu}$ and \hat{z} directions. This rigid transverse DW profile can be fitted by the ansatz $\Omega \equiv \Omega(\eta) = 2 \arctan\{\exp[(q(\eta) - q_0)/\delta]\}$, with $q(\eta) \equiv q_\eta$ being an arbitrary position on the NW, and $q_0 \equiv q(\eta_0)$ defines the position of the DW center, where $\Omega(\eta_0) = \pi/2$. Additionally, $\pi\delta$ is the DW width. From the adopted model, the DW velocity is determined by

$$v = \frac{dq_0}{dt} = -\delta \left(\frac{d\Omega}{dt} \right)_{\Omega=\pi/2}. \quad (1)$$

The magnetization dynamics under an external magnetic field and/or an electric current is described by the Landau-Lifshitz-Gilbert (LLG) equation with spin transfer torque

adiabatic and nonadiabatic terms,

$$\begin{aligned} \frac{d\mathbf{M}}{dt} = & -\gamma\mathbf{M} \times \mathbf{H}_{\text{eff}} + \frac{\alpha}{M_s}\mathbf{M} \times \frac{d\mathbf{M}}{dt} - u \frac{\partial\mathbf{M}}{\partial q_\eta} \\ & + \frac{\beta u}{M_s}\mathbf{M} \times \frac{\partial\mathbf{M}}{\partial q_\eta}, \end{aligned} \quad (2)$$

where γ is the gyromagnetic ratio and α is the damping parameter. Each term of the above equation is associated with the torque produced by effective magnetic fields or currents on the magnetization. The first and second terms on the right side of Eq. (2) are related to the torques produced by the effective field \mathbf{H}_{eff} and the Gilbert damping, respectively. Here, the effective field can be written in a curvilinear basis as $\mathbf{H}_{\text{eff}} = H_{\text{eff}\mu} \hat{\mu} + H_{\text{eff}\eta} \hat{\eta} + H_{\text{eff}z} \hat{z}$. For simplicity, we considered a Permalloy NW, therefore anisotropy vanishes and then \mathbf{H}_{eff} includes the external field \mathbf{H} , and the effective fields produced by exchange \mathbf{H}_{ex} and dipolar \mathbf{H}_{d} interactions, that will be presented after in this text. The third and fourth terms on the right side of Eq. (2) are associated respectively with the adiabatic and non-adiabatic spin transfer torques. Here, β is the phenomenological non-adiabatic spin-transfer parameter, $u = gJ_e\mu_B P/2eM_s$ has velocity dimension and depends on an electric current J_e injected into the magnetic sample, g is the Landé factor, μ_B is the Bohr magneton, P is the spin-polarization factor of the electric current, and e is the electron charge. The adopted magnetic parameters for Permalloy are [18,20,30]: a saturation magnetization $M_s = 813$ erg $\text{G}^{-1} \text{cm}^{-3}$, an exchange stiffness $A = 1.07 \times 10^{-6}$ erg/cm. We use a damping constant $\alpha = 0.01$, and the non-adiabatic spin transfer torque parameter $\beta = 0.04$. Finally, we consider $\pi\delta = 33$ nm, which corresponds to the width of a transverse DW in a NW with a diameter of 30 nm [28].

In the rigid transverse DW model, the LLG equation can be compacted into the form $d\mathbf{M}/dt = -\gamma\mathbf{\Gamma}$, with $\mathbf{\Gamma}$ being the total torque resulting from all relevant interactions acting at the DW center. When written in the (μ, η, z) -coordinate system, the total torque is given by

$$\mathbf{\Gamma}_{\mu,\eta,z} = M_s \begin{bmatrix} -(H_{\text{eff}\eta} + \frac{\alpha}{\gamma}\dot{\Omega} + \frac{\beta u}{\gamma\delta}) \cos \phi \\ H_{\text{eff}\mu} \cos \phi - H_{\text{eff}z} \sin \phi - \frac{\alpha}{\gamma}\dot{\phi} - \frac{u}{\gamma\delta} \\ (H_{\text{eff}\eta} + \frac{\alpha}{\gamma}\dot{\Omega} + \frac{\beta u}{\gamma\delta}) \sin \phi \end{bmatrix}. \quad (3)$$

It is convenient to represent the total torque in a spherical coordinate system (ρ, Ω, ϕ) lying in the curvilinear basis, as depicted in Fig. 1(a). For this purpose, the total torque acting at the DW center can be rewritten as $\mathbf{\Gamma} \equiv \mathbf{\Gamma}_{\rho,\Omega,\phi} = \mathcal{R}(\pi/2, \phi)\mathbf{\Gamma}_{\mu,\eta,z}$, where the transformation matrix $\mathcal{R}(\Omega, \phi)$ reads

$$\mathcal{R}(\Omega, \phi) = \begin{bmatrix} \sin \Omega \sin \phi & \cos \Omega & \sin \Omega \cos \phi \\ \cos \Omega \sin \phi & -\sin \Omega & \cos \Omega \cos \phi \\ \cos \phi & 0 & -\sin \phi \end{bmatrix}.$$

Therefore, the total torque can be expressed as

$$\mathbf{\Gamma}_{\rho,\Omega,\phi} = M_s \begin{bmatrix} 0 \\ H_{\text{eff}z} \sin \phi - H_{\text{eff}\mu} \cos \phi + \frac{\alpha}{\gamma}\dot{\phi} + \frac{u}{\gamma\delta} \\ -(\frac{\alpha}{\gamma}\dot{\Omega} + H_{\text{eff}\eta} + \frac{\beta u}{\gamma\delta}) \end{bmatrix}. \quad (4)$$

From the LLG equation, it is possible to obtain dynamical equations for the angles ϕ and Ω as follows [14]:

$$\dot{\Omega} = -\frac{\gamma}{M_s}\Gamma_\Omega, \quad \dot{\phi} = -\frac{\gamma}{M_s}\Gamma_\phi. \quad (5)$$

Using the expression of DW velocity defined in Eq. (1) and substituting Eq. (4) in Eqs. (5), we obtain

$$\begin{aligned} v &= \frac{\gamma\delta}{1+\alpha^2} \left(\alpha H_{\text{eff}\eta} + \frac{u(1+\alpha\beta)}{\gamma\delta} - \frac{\Gamma_{\text{eff}\eta}}{M_s} \right), \\ \dot{\phi} &= \frac{\gamma}{1+\alpha^2} \left(H_{\text{eff}\eta} + \frac{u(\beta-\alpha)}{\gamma\delta} + \frac{\alpha}{M_s}\Gamma_{\text{eff}\eta} \right), \end{aligned} \quad (6)$$

where $\Gamma_{\text{eff}\eta} = M_s(H_{\text{eff}\mu} \cos \phi - H_{\text{eff}z} \sin \phi)$ is the torque produced by the effective field on the DW center along the η direction.

To perform a complete analysis, we need to determine the dipolar and exchange contributions to \mathbf{H}_{eff} . The dipolar contribution can be obtained by adopting the shape anisotropy approximation: $\mathbf{H}_{\text{d}} = -4\pi(N_\mu M_\mu \hat{\mu} + N_\eta M_\eta \hat{\eta} + N_z M_z \hat{z})$, where N_μ , N_η , and N_z are the demagnetizing factors [31] associated to the $\hat{\mu}$, $\hat{\eta}$, and \hat{z} directions, respectively. The torque produced by \mathbf{H}_{d} on the DW center is evaluated as $\mathbf{\Gamma}_{\text{d}} = -2\pi M_s^2(N_\mu - N_z) \sin(2\phi) \hat{\eta}$. It is worth noting that $N_\mu = N_z$ for NWs with a circular cross section [31] and, consequently, $\mathbf{\Gamma}_{\text{d}} = 0$. This result also applies to a NW with a polygonal cross section with small area [16].

Finally, the exchange effective field is given by [20] $\mathbf{H}_{\text{ex}} = (2A/M_s)\nabla^2\mathbf{m}$, where $\nabla^2\mathbf{m} = \nabla(\nabla \cdot \mathbf{m}) - \nabla \times (\nabla \times \mathbf{m})$ is the Laplacian operator of \mathbf{m} written in the adopted curvilinear system. The explicit equations describing the exchange effective field are presented in the Appendix. All analytical results developed in this section for a head-to-head Néel DW can also be applied to a tail-to-tail DW, just by implementing the transformation $\delta \rightarrow -\delta$.

B. Elliptically bent NW

From the general model described above, we can analyze the DW dynamics in the particular case of an elliptically bent NW whose geometrical description can be done by adopting the following parametrization:

$$x = r \cosh \mu \cos \eta, \quad y = r \sinh \mu \sin \eta. \quad (7)$$

Here $a = r \cosh \mu$ and $b = r \sinh \mu$ are the ellipse semi-axes, with $a \geq b$ and $\mu \geq 0$. When parameter μ is fixed and η varies continuously in the interval $[-\pi, \pi]$, we obtain a complete ellipse. The ellipse eccentricity is intrinsically associated with μ . That is, the greater the value of μ , the smaller the ellipse eccentricity. In this way, the eccentricity vanishes for $\mu \rightarrow \infty$ and the NW geometry presents the shape of a circumference [see Fig. 1(d)]. On the other hand, when η is fixed and μ varies from 0 to ∞ , the parametrization given in Eq. (7) describes a hyperbola segment that orthogonally intersects the associated ellipse. The intersection point defines the localization of the η coordinate on the ellipse [see Fig. 1(b)]. In this context, η determines an arbitrary position along the NW length. The unitary vectors that determine the orthogonal ($\hat{\mu}$) and tangential ($\hat{\eta}$) directions are depicted in Fig. 1(c) for an arbitrary point on the NW. Explicitly, we have $\hat{\mu} = r(\cos \eta \sinh \mu \hat{x} + \sin \eta \cosh \mu \hat{y})/h$ and

$\hat{\eta} = r(-\sin \eta \cosh \mu \hat{x} + \cos \eta \sinh \mu \hat{y})/h$, where the metric factors of the system are

$$h \equiv h_\eta = h_\mu = r \sqrt{\frac{\cosh(2\mu) - \cos(2\eta)}{2}}. \quad (8)$$

To properly describe geometry-induced effects on the DW dynamics, it is convenient to evaluate the ellipse curvature. Following the formalism presented in Ref. [22], we obtain the normalized curvature $\mathcal{C}(\mu, \eta) = \sinh(2\mu)/[\cosh(2\mu) - \cos(2\eta)]$. The behavior of \mathcal{C} is depicted in Fig. 1(e), where we present the local curvature as a function of η for ellipses with fixed perimeter, and $\mu = 0.5$ (red line), $\mu = 1$ (blue-dashed line), and $\mu = 2$ (green line). It can be noticed that in all cases the maximum curvature is associated with $\eta = 0$ and $\eta = \pi$, while the points presenting minimum local curvature values are located at $\eta = \pi/2$ and $\eta = -\pi/2$. Additionally, due to the decrease in the ellipse eccentricity when μ increases, we have that $\lim_{\mu \rightarrow \infty} \mathcal{C} = 1$.

It is important to highlight that in this paper we are not considering a closed elliptical NW, but a section of an ellipse. If the NW were a complete ellipse, we would have a magnetic NW with at least two DWs, an issue out of the scope of our paper. We analyze specifically bent NWs whose associated ellipses have a fixed perimeter $\mathcal{P} = \int_{-\pi}^{\pi} h d\eta = 2000$ nm. Therefore, the NW length L is a fraction of this perimeter that depends on the bounding hyperbola segments characterized by $\eta = \psi$ and $\eta = -\psi$ [see Fig. 1(c)], that is, $L = \int_{-\psi}^{\psi} h d\eta$. In this paper, we consider $\psi = 0.6\pi$, and then η ranges from -0.6π to 0.6π . In this way, the NW length associated with $\mu = 0.5, 1.0, 2.0$, and 4.0 are, respectively, $L \approx 1261$ nm, 1224 nm, 1203 nm, and 1200 nm. It is important to note that parameter r is intrinsically associated with the ellipse semiaxes a and b . Therefore, for a given value of μ and \mathcal{P} , r is implicitly determined.

Now, aiming to perform a more detailed analysis of the dynamics of the system, we determine the exchange effective field acting on the center of a head-to-head Néel DW lying on the elliptic NW. Therefore, from Eqs. (A2)–(A4), we obtain

$$H_{\text{ex}\mu} = -\frac{2A}{M_s} \left\{ 2\mathcal{C}^2(\mu, \eta_0) \left[\frac{\cos(2\eta_0) + \cosh(2\mu)}{r^2 \sinh^2(2\mu)} \sin \phi - \frac{\text{sech}\mu}{r\delta} \sqrt{1 + \text{csch}^2\mu \sin^2 \eta_0} \right] + \frac{\sin \phi}{\delta^2} \right\}, \quad (9)$$

$$H_{\text{ex}\eta} = -2\sqrt{2} \sin(2\eta_0) \frac{A}{M_s r \delta} \left(\frac{\mathcal{C}(\mu, \eta_0)}{\sinh(2\mu)} \right)^{3/2} \quad (10)$$

and

$$H_{\text{ex}z} = -\frac{2A}{M_s \delta^2} \cos \phi, \quad (11)$$

where $\mathcal{C}(\mu, \eta_0)$ is the local normalized curvature of the ellipse, evaluated at $\eta = \eta_0$ (DW center position) for a given μ . Therefore, one can conclude that in addition to the normal component $H_{\text{ex}\mu}$ and the component $H_{\text{ex}z}$ of the exchange effective fields (as we observed for DWs on a circularly bent NW [20]), here we also obtain a tangential component of the exchange effective field $H_{\text{ex}\eta}$. This tangential field emerges from the exchange-driven curvature-induced effective interactions [22] and vanishes at the positions with maximum and

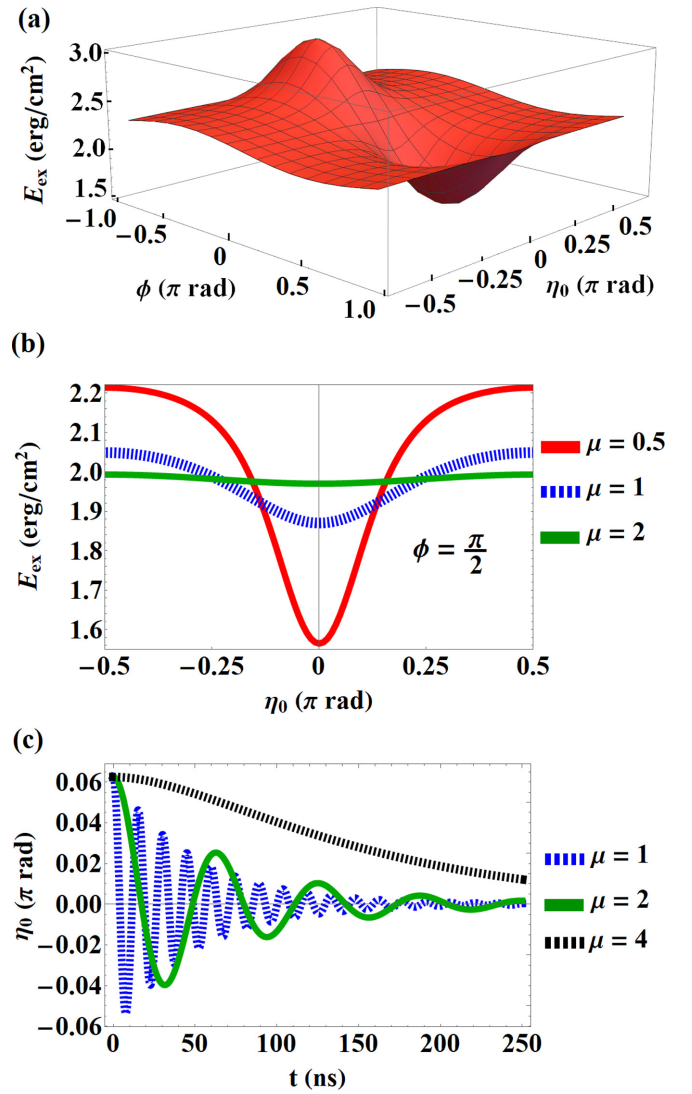


FIG. 2. (a) Exchange energy E_{ex} as a function of the DW position η_0 and phase ϕ for an elliptical NW with $\mu = 0.5$. (b) Behavior of E_{ex} as a function of the DW position η_0 for $\phi = \pi/2$. (c) Behavior of the DW in the absence of external stimuli developing harmonic decaying oscillations around $\eta_0 = 0$.

minimum curvatures along the NW length. Because the position with minimum curvature represents the point at which the DW presents its maximum energy [see Fig. 2(b)], it is an unstable equilibrium point. Therefore, $H_{\text{ex}\eta}$ is responsible for inducing a DW motion along the NW even in the absence of external stimuli, bringing it to the stable equilibrium position at the maximum curvature point. This DW pinning has been previously described by Yershov *et al.* [27]. Finally, as expected, one can notice that for a circular geometry with radius R ($\mu \rightarrow \infty$), which presents a constant curvature, there is no exchange-driven tangent effective field, that is,

$$\lim_{\mu \rightarrow \infty} H_{\text{ex}\mu} = \frac{2A}{M_s} \left[\frac{2}{R\delta} - \left(\frac{1}{\delta^2} + \frac{1}{R^2} \right) \sin \phi \right], \quad (12a)$$

$$\lim_{\mu \rightarrow \infty} H_{\text{ex}\eta} = 0, \quad \text{and} \quad \lim_{\mu \rightarrow \infty} H_{\text{ex}z} = -\frac{2A}{M_s \delta^2} \cos \phi. \quad (12b)$$

III. DW DYNAMICS IN THE ABSENCE OF EXTERNAL STIMULI

Aiming at having some preliminary perspectives on the DW dynamics, we analyze the DW energy as a function of its position (η_0) and phase (ϕ) along the NW in the absence of external stimuli. As previously reported in bent NWs with circular cross sections [17,27], the main contribution to the total energy responsible for the DW dynamic behavior is the exchange interaction, given by $E_{\text{ex}} = \int_{\text{NW}} \mathcal{E}_{\text{ex}} d\eta$, where $\mathcal{E}_{\text{ex}} = -(1/2)\mathbf{M} \cdot \mathbf{H}_{\text{ex}}$ is the exchange energy density and the integral is performed over the NW length. Numerical results for E_{ex} as a function of η are depicted in Fig. 2(a), for $\mu = 0.5$. One can notice that the minimum energy is obtained when the DW is located at $\eta_0 = 0$ (the curvature maximum) and $\phi = \pi/2$ (DW center is pointing outward of the bend). Additionally, the maximum energy points corresponds to a DW at $\eta_0 = \pm\pi/2$ (minimum curvature points) and $\phi = -\pi/2$ (DW pointing inward of the bend). Therefore, one can conclude that $\eta_0 = 0$ and $\phi = \pi/2$ represent the equilibrium configuration for the DW, in agreement with results presented in Ref. [27]. We have also analyzed the influence of the ellipse eccentricity on the DW exchange energy in the specific case where the DW phase is $\phi = \pi/2$. Main results are depicted in Fig. 2(b) for NWs with $\mu = 0.5$ (red line), $\mu = 1.0$ (blue-dashed line), and $\mu = 2.0$ (green line). It can be noticed that the potential well around $\eta_0 = 0$ and $\phi = \pi/2$ becomes deeper for more eccentric ellipses and vanishes for large μ values.

In the absence of external stimuli ($H = 0$ and $u = 0$), the DW motion is purely determined by the action of a curvature-induced effective field and the damping effects. By considering that the DW is initially near the maximum curvature point, we numerically solved Eqs. (6) to analyze the DW position and phase as a function of time. Main results are illustrated in Fig. 2(c), from which it is possible to verify that the DW describes harmonic decaying oscillations, reaching its equilibrium position at $\eta_0 = 0$ and $\phi = \pi/2$.

The observed harmonic damped oscillations are associated with the existence of a exchange-driven curvature-induced effective field, which works as a restoring field that tends to bring the system to its equilibrium position. This restoring field can be determined by expanding the tangential component of the exchange field for small displacements around $\eta = 0$, obtaining the so-called harmonic approximation to the tangential exchange field ($H_{\text{ex}\eta}^{\text{HA}}$). Therefore, from Eq. (10), we obtain

$$H_{\text{ex}\eta}^{\text{HA}} = -\kappa_{\mu}\eta_0, \quad \kappa_{\mu} = \frac{2A}{M_s r \delta} \text{csch}^3 \mu. \quad (13)$$

Figure 3 illustrates the behavior of $H_{\text{ex}\eta}$ (blue line) as a function of η_0 for NWs with different eccentricities. A linear fit of $H_{\text{ex}\eta}^{\text{HA}}$ (red-dashed line) evidences that the magnitude of $H_{\text{ex}\eta}$ increases as a function of η_0 inside the interval $[-\eta_e, \eta_e]$ (black lines), and in this case, the DW moves under the so-called elastic regime. We observe that the harmonic approximation for the restoring field agrees well with $H_{\text{ex}\eta}$ even for displacements $\eta_0 \sim 0.1\pi$ rad. Nevertheless, beyond the elastic regime $H_{\text{ex}\eta}$ decreases with η_0 and the harmonic approximation cannot be used to describe the DW motion.

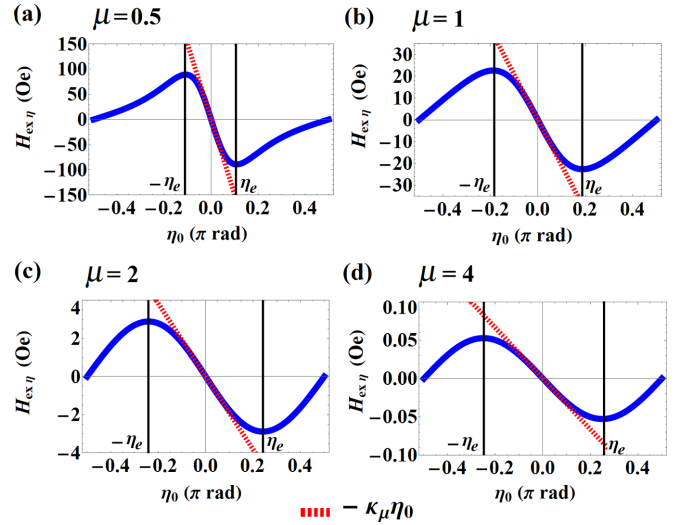


FIG. 3. Tangent exchange field $H_{\text{ex}\eta}$ as a function of the DW position η_0 for $\mu = 0.5$ (a), $\mu = 1.0$ (b), $\mu = 2.0$ (c), and $\mu = 4.0$ (d). The black vertical lines delimit the elastic regime in which the magnitude of $H_{\text{ex}\eta}$ increases with η_0 . The dashed red line depicts the fitting of the harmonic approximation ($H_{\text{ex}\eta}^{\text{HA}}$) for small DW displacements.

One can also notice that the strength of $H_{\text{ex}\eta}$ increase as μ decreases.

The above-described results suggest that we can write a dynamic equation for the DW motion in an analogy with a damped harmonic oscillator. That is, under the absence of external stimuli, the DW moves around the point of maximum curvature analogously to a mass-spring system (see Fig. 4). Therefore, when the DW displaces in a region where the linear regime is valid, it moves under the action of a restoring field, which vanishes in the position of the NW having maximum curvature. In this case, κ_{μ} can be interpreted as an elastic constant that increases with the NW eccentricity. For describing the DW dynamics, we focus on the ϕ component of the torque given in Eq. (4), which is responsible for the fields that have components along the direction tangent to the NW. Because $H = 0$ and $u = 0$, we obtain that $\Gamma_{\phi} = -M_s[(\alpha/\gamma)\dot{\Omega} + H_{\text{ex}\eta}]$, where $\dot{\Omega} = -(h/\delta)\dot{\eta}_0$. In this case, the only fields acting along the η direction are H_{ex}

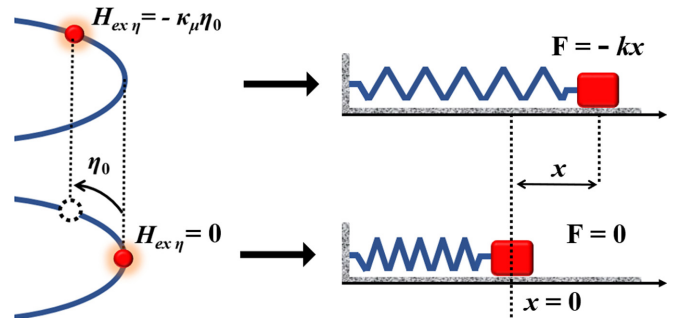


FIG. 4. Analogy between the DW motion in a bent NW and a mass-spring system. A DW in the point of maximum curvature corresponds to the spring without deformation. Red dots represent the DW center.

and $-(\alpha h/\gamma\delta)\dot{\eta}_0$. Thus, for small displacements around the point of maximum curvature, we can assume that the DW propagates following Newton's second law. This assumption allows us to write

$$m\ddot{\eta}_0 = -\kappa_\mu\eta_0 - b_\mu\dot{\eta}_0, \quad (14)$$

where m can be interpreted as a DW effective inertial term. Additionally, $b_\mu = (\alpha/\gamma\delta)h \approx (\alpha/\gamma\delta)r \sinh\mu$. The formal solution of Eq. (14) is

$$\eta_0(t) = e^{-t\beta_\mu} (C_1 e^{t\sqrt{\beta_\mu^2 - \omega_0^2}} + C_2 e^{-t\sqrt{\beta_\mu^2 - \omega_0^2}}), \quad (15)$$

where $\beta_\mu = b_\mu/2m$ is the damping factor, $\omega_0 = \sqrt{\kappa_\mu/m}$ is the natural frequency of the system, that is, the frequency that the oscillator would present in the absence of damping. The constants C_1 and C_2 can be determined from the initial conditions. For a complete description of the oscillatory character of the DW motion, we need to determine ω_0 from the solutions of Eqs. (6) in the absence of external stimuli and consider $\alpha = 0$. Under these assumptions, for small displacements around $\eta = 0$ and $\phi = \pi/2$, we obtain the DW position as $\eta_0(t) = c_1 e^{i\omega_0 t} + c_2 e^{-i\omega_0 t}$, with ω_0 given by

$$\omega_0 = \frac{2A\gamma}{M_s r^2 \sinh^3 \mu} \sqrt{\frac{2r}{\delta} \cosh\mu - \coth^2 \mu}. \quad (16)$$

It is worth noting that ω_0 depends only on intrinsic magnetic and geometric parameters of the NW. As expected, due to the decrease of κ_μ as a function of μ , the natural frequency of the system decreases when the ellipse eccentricity decreases, in such a way that the DW oscillatory frequency practically vanishes for $\mu \approx 4$. From the adopted analogy, we define the DW effective inertial term as $m = \kappa_\mu/\omega_0^2$, resulting in

$$m = \frac{M_s r^3 \sinh^3 \mu}{2A\gamma^2 \delta \left(\frac{2r}{\delta} \cosh\mu - \coth^2 \mu\right)}. \quad (17)$$

One can observe that m increases asymptotically as a function of μ , reaching the maximum value $\lim_{\mu \rightarrow \infty} m = M_s \mathcal{P}^3 / [16A\pi^2 \gamma^2 (\mathcal{P} - \pi\delta)] \approx 6.3 \times 10^{-16} \text{ Oe} \times \text{s}^2$ for $\mu \gtrsim 4$ (circularly bent NW with curvature radius R). We highlight that the adopted analogy considers the curvature-induced magnetic field as the effective force acting on the DW, and then this inertial term has the dimension of $\text{Oe} \times \text{s}^2$. Nevertheless, one can obtain the DW mass in kg by observing that $M_s H/R$ corresponds to the effective tangential force per volume acting on the DW center in an NW with $\mu \gtrsim 4$. Furthermore, $R\ddot{\eta}_0$ is the tangential acceleration. Thus, the mass per volume, \mathcal{M} , is given by $\mathcal{M} = m(M_s/R^2)$, and the estimated DW mass is $\mathcal{M}V_{\text{DW}} = 1.3 \times 10^{-23} \text{ kg}$, where V_{DW} is the DW volume. One can observe that the obtained value is of the same order as other theoretical [19] and experimental [32] predictions previously reported for thicker wires. Another important point to be highlighted is that the here-used inertia-based DW mass definition is fundamentally different from the usual mass determined by Döring [33], who used the Lagrangian formulation to determine the velocity-dependent micromagnetic DW energy [19,33,34]. Finally, it is also worth noticing that the obtained expression for the DW inertial term is not valid for $\mu \lesssim 0.1$. In this case, ω_0 and m present discontinuities due to the very large eccentricity of the elliptical

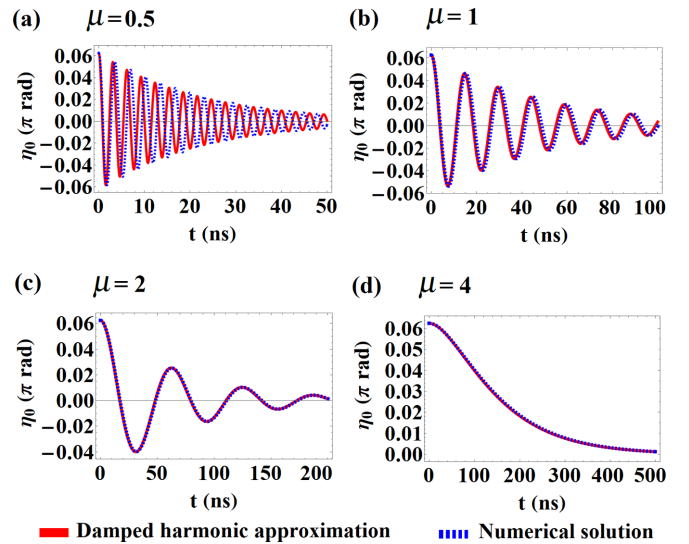


FIG. 5. Weak damped oscillations for $\mu = 0.5$ (a), $\mu = 1$ (b), and $\mu = 2$ (c). The strong damped regime is depicted in (d) for $\mu = 4$. Here, red lines are the solution obtained using the harmonic approximation, while the dashed blue lines are the solutions obtained from the numerical evaluation of the complete dynamics equations. The DW starts from the rest at the position $\eta = \pi/16$.

NW, where the rigid transverse DW assumption is not valid anymore.

Now, to better understand the DW motion described by Eq. (15), we can perform an analysis for two particular cases regarding the damping. These two cases can be separated by the critical damping $\beta_\mu = \omega_0$, value at which the system returns to the steady state as quickly as possible, with no oscillations. First, we investigate the underdamped regime (UD), which occurs for $\beta_\mu < \omega_0$, characterized by oscillations with amplitude gradually decreasing to zero. In this case, the formal solution given by Eq. (15) can be expressed as damped periodic oscillations described by

$$\eta_0(t) = \mathcal{A} e^{-t\beta_\mu} \cos(t\sqrt{\omega_0^2 - \beta_\mu^2} - \zeta), \quad (18)$$

where $\mathcal{A} = \eta_0(0) \sec \zeta$. Assuming $\dot{\eta}_0(0) = 0$ as the initial condition, we obtain $\zeta = \arccos(\sqrt{\omega_0^2 - \beta_\mu^2}/\omega_0)$. In the elastic regime, there are positions occupied by the DW where the linear relation between $H_{\text{ex}\eta}$ and η is not valid. Therefore, we compare the DW position obtained from the UD harmonic oscillator approach with that predicted by the LLG equation. For this purpose, we obtain the behavior of $\eta_0(t)$ from both the analytical approach given by Eq. (18) and the numerical solution of Eqs. (6) under initial conditions $\eta_0(0) = \pi/16$ and $\phi(0) = \pi/2$. Our results are depicted in Figs. 5(a)–5(c) for $\mu = 0.5, 1$, and 2 , respectively. One can observe that the comparison between the harmonic oscillator analogy (red line) and the numerical solution of the LLG equation (blue-dashed line) evidences excellent agreement for $\mu = 1$ and $\mu = 2$. However, for $\mu = 0.5$, the frequencies obtained from these two solutions are slightly different in such a way that the predicted DW positions are different. This difference occurs because the length $\Delta\eta_e$ of the elastic regime diminishes as μ decreases (see Fig. 3). Therefore, a better agreement

between the harmonic analogy and the numerical solution of LLG emerges if we consider a smaller initial amplitude. Additionally, our results also evidence the decrease in the DW oscillation frequency as a function of μ . That is, the smaller is the ellipse eccentricity, the lower is the DW oscillatory frequency.

The second case we can analyze is the overdamped regime (OD), which is obtained for $\beta_\mu > \omega_0$. In this case, the DW coordinate exponentially decays to the equilibrium position with no oscillations. To better understand this OD regime, we need to determine the constants C_1 and C_2 in Eq. (15). Therefore, assuming as initial condition $\dot{\eta}_0(0) = 0$, we obtain

$$C_1 = \frac{\eta_0(0)}{2} \left(1 + \frac{\beta_\mu}{\sqrt{\beta_\mu^2 - \omega_0^2}} \right), \quad (19a)$$

$$C_2 = \frac{\eta_0(0)}{2} \left(1 - \frac{\beta_\mu}{\sqrt{\beta_\mu^2 - \omega_0^2}} \right). \quad (19b)$$

We have also compared the results obtained from the damping oscillation approach and the numerical solution of the LLG equation. The results obtained for $\mu = 4$, with initial conditions $\eta_0(0) = \pi/16$ and $\phi(0) = \pi/2$, are depicted in Fig. 5(d), where one can notice that the DW goes to its equilibrium position with no oscillations. Therefore, one conclude that the ellipse eccentricity determines the coefficient of the exponential decay of the DW position.

It can be observed that the UD and the OD regimes are separated by a critical damping factor $\beta_\mu = \omega_0$. This relation allows us to find the Gilbert damping of the magnetic NW from the following expression

$$\alpha = \frac{4\gamma A \text{csch}^4 \mu_c}{M_s r^2 \omega_0}, \quad (20)$$

where μ_c is associated with the ellipse eccentricity that separates the UD and the OD regimes. Therefore, although there are different methodologies to evaluate the value of α , Eq. (20) provides an interesting alternative for experimental determination of the Gilbert damping factor of a magnetic NW. That is, by varying the ellipse eccentricity and analyzing the DW oscillations, one can look for the approximated value of μ_c that produces a transition between the UD and OD regimes. When μ_c is obtained, Eq. (20) can be used to determine a valid α value.

We highlight that although the damping factor obtained from the mechanical analogy (β) depends on α , one cannot interpret the damping parameter of the magnetic system as static or dynamic friction coefficients of its mechanical counterpart. Additionally, the phenomenology described here could also be analyzed from an analogy with other damped harmonic systems, such as, for instance, a simple pendulum in a gravity field [32].

IV. DW DYNAMICS UNDER A SPIN POLARIZED ELECTRIC CURRENT

After analyzing the oscillatory behavior of a DW displacing in an elliptical NW in the absence of external stimuli, we can describe the effects that electric currents or mag-

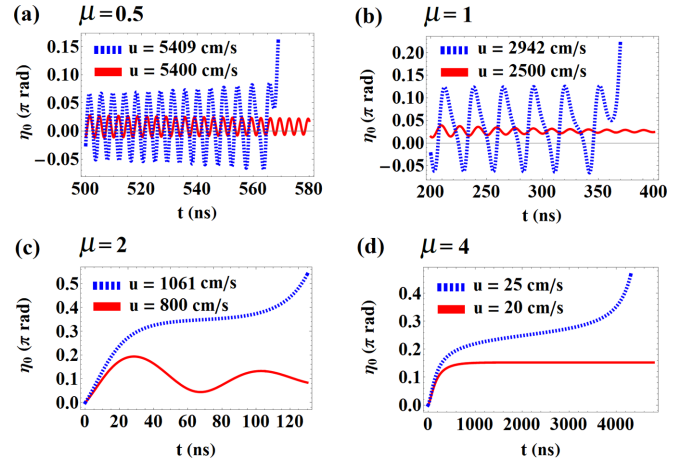


FIG. 6. The DW angular position as a function of time for different electric current intensities (which corresponds to different u values) for NWs with $\mu = 0.5$ (a), $\mu = 1$ (b), $\mu = 2$ (c), and $\mu = 4$ (d). Red lines depict the dynamics in the pinning state, while the dashed blue lines refers to the unpinning DW.

netic fields generate on the DW dynamics. The extra torque produced on the DW due to the inclusion of an external stimulus can be used for two main purposes: to control the DW stationary position, or to unpin the DW with the aim to propagate it further from the region of maximum curvature.

Because most of technological propositions demanding the control of the magnetization properties consider current-driven mechanisms, we will start analyzing the effects of the application of an electric current on the properties of a DW displacing in an elliptical NW. It is worth noticing that considered NW consists of a curvilinear system that does not present torsion. Therefore, there is no effect on the adiabatic and non-adiabatic terms of the LLG equation that changes the behavior of the DW dynamics [19]. Additionally, we are dealing with a magnetic system within the limit of high magnetic moments and with sizes much larger than the lattice spacing. In this context, we expect that the conduction electrons behave as in the model proposed by Zhang and Li [35], where their magnetic moments are almost parallel to the position-dependent NW magnetization.

The analysis of Eqs. (6) reveals that the current acts in a different way on the translation and on the rotation motions of the DW. That is, current acts as an effective field $u(1 + \alpha\beta)/(\alpha\gamma\delta)$ that influences the DW translation velocity v . But the rotation of the DW around the NW axis is affected by a different current-induced effective field, given by $u(\beta - \alpha)/(\gamma\delta)$. This asymmetry in the current effects on the translation and rotation motions of the DW does not allow us to obtain analytical solutions for the DW position and phase. However, we can develop a numerical analysis of Eqs. (6). Results for the DW position are depicted in Fig. 6, considering four different values of μ and two values of the electric current for each case. It can be noticed that depending on the current strength, the DW changes its stationary position or is unpinned from the region of maximum curvature, moving in an oscillatory motion far from this position. Red

lines represent the DW position under the action of a current small enough to keep the DW pinned around a region near to the maximum curvature. In this case, the DW follows a harmonic damped oscillation around this position, where the electric current balances the effective field. The analysis of Fig. 6 also reveals that the NW eccentricity influences the frequency, amplitude, and the kind of damped harmonic oscillation (UD or OD). The greater the eccentricity, the greater the oscillation frequency. If the DW is under the action of an electric current that overcomes a threshold value (blue-dashed lines), the DW escapes from the “potential well” generated by the exchange-driven curvature-induced effective field. We can observe that before being unpinned from the stationary position, the DW oscillates around it with a frequency that decreases as a function of μ . Finally, we observe that the amplitude of the oscillations increases with the electric current. Because we have no analytical solutions for describing the DW position as a function of the electric current, the critical values presented in Fig 6 were numerically obtained in a trial and error procedure.

We call attention to the fact that high temperature effects could change the phenomenology described here. Indeed, the effect of temperature plays a role in the current-driven DW motion in such a way that Joule heating influence the DW behavior because it changes the magnetic parameters of the NW and decrease the critical fields. For instance, the emergence of spin waves or multiple DWs induced by temperature can assist or act against the pure spin-transfer torque [36,37]. In the same hand, when the DW is under the action of a threshold current dividing linear and oscillatory dynamical regimes, the thermal field appearing due to Joule heating can suppress the Walker breakdown and accelerates the DW propagation [38,39]. Therefore, if temperature effects are considered in describing the DW dynamics in bent NWs, one could expect that the threshold current for which the DW is unpinned should diminish. Additionally, after unpinned, the oscillatory motion of the DW could be suppressed. However, most of these effects occur for temperatures higher than 300 K.

V. DW DYNAMICS UNDER THE ACTION OF A TANGENTIAL MAGNETIC FIELD

Due to the asymmetric role played by the spin transfer torque term on the translation and rotation motion, our analysis of the DW motion under electric current is strictly numeric. Therefore, to obtain analytical solutions and better describe the dynamical properties of a DW displacing in an elliptically-bent NW under the action of external stimulus, we consider now that the system is subject to an external magnetic field $\mathbf{H} = H\hat{\eta}$, *i.e.*, it is an inhomogeneous field whose field lines follow the curvature of the wire. Although there are experimental difficulties for implementing such a field, our main purpose here is to obtain analytical results that allows us to obtain a description of the DW unpinning phenomenon.

From considering our analogy with a spring-mass system, a tangential magnetic field $\mathbf{H} = H\hat{\eta}$ applied on the NW can be considered as an extra “force” term associated with the external magnetic field in the “Newton’s law” (14) that describes

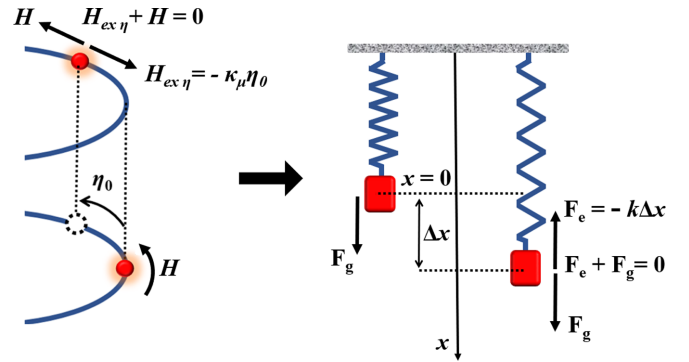


FIG. 7. Analogy between the DW motion under the action of a tangential external magnetic field and a mass-spring system under the action of the gravitational force. Red dots represent the DW center. The external magnetic field is responsible for bringing the DW to a new equilibrium point.

the DW motion

$$m\ddot{\eta}_0 = H - \kappa_\mu \eta_0 - b_\mu \dot{\eta}_0. \quad (21)$$

One can notice that the external field plays a role similar to the gravitational force acting on a mass-spring system (see Fig. 7). Therefore, the DW assumes a new equilibrium position that depends on the magnetic field strength H and the curvature-induced effective field $H_{ex\eta}$, which compete with each other. From Eq. (21), we obtain

$$\eta_0(t) = e^{-t\beta_\mu} (\mathcal{K}_1 e^{-t\sqrt{\beta_\mu^2 - \omega_0^2}} + \mathcal{K}_2 e^{t\sqrt{\beta_\mu^2 - \omega_0^2}}) + \eta_H \quad (22)$$

where $\eta_H = \frac{HM_s r \delta \sinh^3 \mu}{2A}$. Assuming that the initial conditions are $\eta_0(0) = 0$ and $\dot{\eta}_0(0) = 0$, the constants \mathcal{K}_1 and \mathcal{K}_2 are evaluated as

$$\mathcal{K}_1 = -\frac{\eta_H}{2} \left(1 - \frac{\beta_\mu}{\sqrt{\beta_\mu^2 - \omega_0^2}} \right), \quad (23a)$$

$$\mathcal{K}_2 = -\frac{\eta_H}{2} \left(1 + \frac{\beta_\mu}{\sqrt{\beta_\mu^2 - \omega_0^2}} \right). \quad (23b)$$

As expected, the analysis of Eq. (22) reveals that the DW presents a damped oscillatory motion around a new equilibrium position η_H that depends on the external magnetic field and the ellipse eccentricity. We can observe that, for a given H , the equilibrium position is farther from $\eta = 0$ for NW with lower eccentricity. This behavior is intrinsically associated with the decrease in $H_{ex\eta}$ when μ increases. In this context, we can again classify the DW motion under the action of an external magnetic field as UD or OD, for $\beta_\mu < \omega_0$ or $\beta_\mu > \omega_0$, respectively. Previous statements can be corroborated from the analysis of Fig. 8, which illustrates the DW position as a function of time obtained from both Eq. (22) (red lines) and numerical solutions of Eqs. (6) (blue-dashed lines). Good agreement between both methods is observed. Again, DWs moving in elliptical NWs with $\mu = 0.5$, $\mu = 1$, and $\mu = 2$ present a UD regime, while OD behavior is obtained for $\mu = 4$.

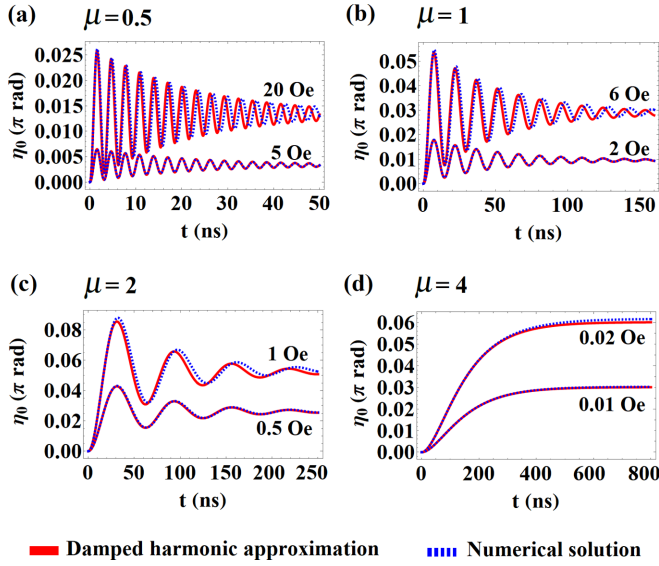


FIG. 8. UD regime to the DW oscillations for $\mu = 0.5$ (a), $\mu = 1$ (b), and $\mu = 2$ (c). The OD regime is depicted in (d) for $\mu = 4$. Here, red lines are the solution described by the harmonic approximation, while the blue-dashed lines are the solutions described by the numerical evaluation of the LLG equation.

As stated before, $H_{ex\eta}$ increases with η_0 in the interval $[-\eta_e, \eta_e]$, but decreases when η_0 is beyond this region (see Fig. 3). Therefore, there is a threshold for the external magnetic field from which the elastic regime is not more valid and the DW is unpinned from the position with maximum curvature. The limit field ensuring that the DW does not exceed the elastic regime can be estimated as $H_e \approx -H_{ex\eta}(\eta_e/2)$ in such a way that the DW equilibrium position is $\eta_0 = \eta_e/2$. In this case, in the first oscillation, the DW displaces $\Delta\eta_0 \approx \eta_e/2$ beyond the equilibrium position and then the DW does not overcome the elastic limit. After some algebra, H_e can be evaluated as

$$H_e \approx \frac{4A\sqrt{2 + 2\cosh(2\mu)} - \lambda}{M_s r \delta (2\cosh(2\mu) - \sqrt{2 - 2\cosh(2\mu)} + \lambda)^{3/2}}, \quad (24)$$

where $\lambda = \sqrt{14 + 2\cosh(4\mu)}$. Equation (24) allows us to estimate H_e as a function of the NW eccentricity. For instance, $H_e \approx 68.15$ and 16.87 Oe for $\mu = 0.5$ and 1 , respectively. To analyze the DW behavior for different external magnetic fields and NW eccentricities, we determine the DW position and phase for elliptically bent NWs with eccentricities $\mu = 0.5$ and $\mu = 1$. The obtained results are depicted in Fig. 9, where red lines represent the DW position and phase when it is under the action of the $H = H_e$. In this case, the DW reaches a new equilibrium position depending on the NW eccentricity, given by $\eta_e/2 \approx 0.05\pi$ and 0.1π rad for $\mu = 0.5$ and 1 , respectively. We also highlight that the DW does not overcome the position η_e , delimiting the elastic regime (see black-dashed lines in Fig. 9). The green-dotted lines in Fig. 9 show the DW position when it is under the action of a magnetic field whose strength is slightly higher than H_e . In this case, during its oscillations, the DW reaches a position along the NW that is out of the range in which the elastic regime occurs. Nevertheless, it is noteworthy that even if the DW exceeds position η_e during

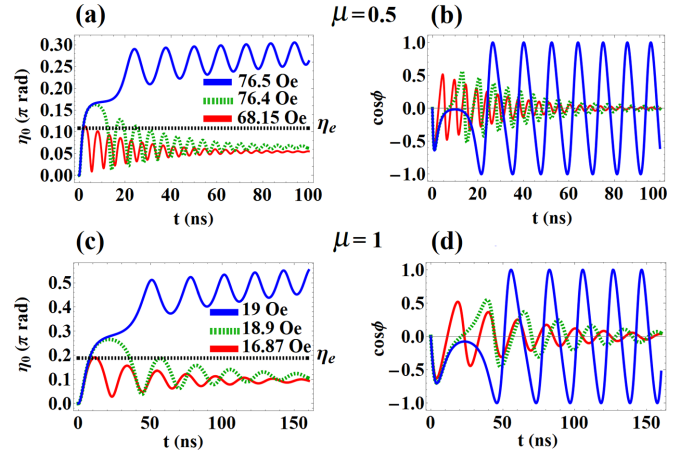


FIG. 9. (a) The DW angular position along the time for a NW with $\mu = 0.5$ different intensities of the Zeeman field. (b) The $\cos \phi$ as a function of time under the same fields as case (a). (c) DW angular position along the time for a NW with $\mu = 1$ under different intensities of the Zeeman field. (d) The $\cos \phi$ as a function of time under the same fields as case (c).

the first oscillation, the curvature-induced tangential effective field is still big enough to ensure that $|H_{ex\eta}| > |H|$, which brings the DW back to a position where $\eta_0 < \eta_e$. Finally, if the magnetic field overcomes a threshold, the DW is unpinned and starts propagating along the NW in an oscillatory motion followed by a DW rotation. This behavior is depicted by blue lines in Fig. 9, where the critical magnetic field is numerically evaluated.

We highlight that the analysis of the DW phase yields a completely analogous behavior to that obtained for the DW position [see Figs. 9(b) and 9(d)]. In this case, while the DW translation motion behaves like a mass-spring system in the elastic regime, we observe that in its rotational dynamics, the DW behaves as a torsion pendulum. Furthermore, the natural frequency ω_0 and the damping parameter β_μ are the same as obtained for the DW translational motion.

VI. CONCLUSIONS

In this paper, we developed an analysis of a transverse domain wall dynamics displacing along an elliptically bent NW with circular cross section. The curvature gradient of the elliptical geometry strongly affects the DW translation and rotation motions. Particularly, the exchange-driven curvature-induced tangential effective field produces a pinning potential, which increases with the ellipse eccentricity and traps the DW near the region presenting maximum curvature. The DW equilibrium position is a result of the competition between the tangential effective field and the torque on the magnetization originated from an external stimulus (electric current or magnetic field). Our results evidence that if the external stimuli are below a threshold value, the DW moves following a damped harmonic oscillation around an equilibrium position. Nevertheless, if the external stimulus overcomes the threshold imposed by the exchange-driven curvature-induced tangential effective field, the DW is unpinned from the region with maximum curvature and moves along the NW with an oscillatory

motion characteristic of the Walker regime. Therefore, the results here presented support the possibility of controlling the DW dynamics by varying both the NW curvature and external stimulus.

ACKNOWLEDGMENTS

In Brazil, we thank the financial support of Capes (Finance Code No. 001), Fapemig (Grant No. APQ-00648-22), and CNPq (Grant No. 302084/2019-3). D.A. acknowledges financial support from Financiamento Basal para Centros Científicos y Tecnológicos under Project No. AFB180001, and Fondecyt No. 1220215. V.L.C.-S. acknowledges the hospitality of the Cedenna under Project No. AFB180001 and the University of Santiago de Chile. The work of O.C.-F. was supported by Grant No. PID2019-108075RB-C31 funded by MCIN/AEI/No. 10.13039/501100011033. R.M. acknowledges the Natural Environment Research Council (Grant No. NE/001018/1).

APPENDIX: EXPRESSIONS FOR THE EXCHANGE ENERGY DENSITY AND EXCHANGE FIELD IN AN ARBITRARY CURVILINEAR NW

The exchange energy can be calculated as $E_{\text{ex}} = \int_{\text{NW}} \mathcal{E}_{\text{ex}} h_{\eta} d\eta$, where $\mathcal{E}_{\text{ex}} = -(1/2)\mathbf{M} \cdot \mathbf{H}_{\text{ex}}$ is the exchange energy density and $\mathbf{H}_{\text{ex}} = (2A/M_s)\nabla^2 \mathbf{m}$ is the exchange effective field evaluated in an arbitrary point on the NW length. Under this framework, we assume that the magnetization varies only along to the tangential direction, that is, $\mathbf{m} = \mathbf{m}(\eta)$, and then the DW is described by $\Omega = \Omega(\eta)$. Furthermore, we recall that the considered NW lies in the xy plane, which implies $h_z = 1$. Thus, we can determine an expression for the exchange density energy in a transverse DW lying in a general curvilinear system (μ, η, z) as follows:

$$\begin{aligned} \mathcal{E}_{\text{ex}} = A \left\{ \left(\frac{1}{h_{\eta}} \frac{\partial \Omega}{\partial \eta} \right)^2 - \frac{2}{h_{\mu} h_{\eta}^2} \frac{\partial h_{\eta}}{\partial \mu} \frac{\partial \Omega}{\partial \eta} \sin \phi \right. \\ + \frac{3 - \cos(2\phi) + 2 \cos(2\Omega) \cos^2 \phi}{4h_{\mu}^2 h_{\eta}^2} \\ \times \left[\left(\frac{\partial h_{\mu}}{\partial \eta} \right)^2 + \left(\frac{\partial h_{\eta}}{\partial \mu} \right)^2 - h_{\eta} \frac{\partial^2 h_{\eta}}{\partial \mu^2} \right] \\ + \frac{3 + \cos(2\Omega) - 2 \sin^2 \Omega \cos(2\phi)}{4h_{\mu} h_{\eta}^3} \\ \times \left(\frac{\partial h_{\mu}}{\partial \eta} \frac{\partial h_{\eta}}{\partial \eta} - h_{\eta} \frac{\partial^2 h_{\mu}}{\partial \eta^2} \right) \\ \left. + \frac{1}{h_{\mu}^3 h_{\eta}} \frac{\partial h_{\mu}}{\partial \mu} \frac{\partial h_{\eta}}{\partial \mu} (\cos^2 \Omega + \sin^2 \Omega \sin^2 \phi) \right\}. \quad (\text{A1}) \end{aligned}$$

It is also useful to determine an expression for the exchange effective field acting on the center of a DW lying in a bent NW. For this purpose, we need to calculate the Laplacian operator of \mathbf{m} and evaluate it for $\Omega = \pi/2$. Specifically, for a head-to-head DW, we have

$$\begin{aligned} H_{\text{ex}\mu} &\equiv (\mathbf{H}_{\text{ex}} \cdot \hat{\mu})_{\Omega=\pi/2} \\ &= -\frac{2A}{M_s} \left\{ \left[\frac{1}{\delta^2} + \left(\frac{1}{h_{\mu} h_{\eta}} \frac{\partial h_{\mu}}{\partial \eta} \right)^2 + \left(\frac{1}{h_{\mu} h_{\eta}} \frac{\partial h_{\eta}}{\partial \mu} \right)^2 \right. \right. \\ &\quad + \frac{1}{h_{\mu} h_{\eta}^3} \frac{\partial h_{\mu}}{\partial \eta} \frac{\partial h_{\eta}}{\partial \eta} + \frac{1}{h_{\mu}^3 h_{\eta}} \frac{\partial h_{\mu}}{\partial \mu} \frac{\partial h_{\eta}}{\partial \mu} \\ &\quad \left. \left. - \frac{1}{h_{\mu} h_{\eta}^2} \frac{\partial^2 h_{\mu}}{\partial \eta^2} - \frac{1}{h_{\mu}^2 h_{\eta}} \frac{\partial^2 h_{\eta}}{\partial \mu^2} \right] \sin \phi - \frac{2}{\delta h_{\mu} h_{\eta}} \frac{\partial h_{\eta}}{\partial \mu} \right\}, \quad (\text{A2}) \end{aligned}$$

$$\begin{aligned} H_{\text{ex}\eta} &\equiv (\mathbf{H}_{\text{ex}} \cdot \hat{\eta})_{\Omega=\pi/2} \\ &= -\frac{2A}{M_s} \left\{ \left[\frac{1}{h_{\mu} h_{\eta}^3} \frac{\partial h_{\eta}}{\partial \eta} \frac{\partial h_{\eta}}{\partial \mu} - \frac{1}{h_{\mu}^3 h_{\eta}} \frac{\partial h_{\mu}}{\partial \eta} \frac{\partial h_{\mu}}{\partial \mu} \right. \right. \\ &\quad + \frac{1}{h_{\mu}^2 h_{\eta}} \frac{\partial}{\partial \mu} \left(\frac{\partial h_{\mu}}{\partial \eta} \right) \\ &\quad \left. \left. - \frac{1}{h_{\mu} h_{\eta}^2} \frac{\partial}{\partial \mu} \left(\frac{\partial h_{\eta}}{\partial \eta} \right) \right] \sin \phi + \frac{1}{\delta h_{\mu} h_{\eta}} \frac{\partial h_{\mu}}{\partial \eta} \right\}, \quad (\text{A3}) \end{aligned}$$

and

$$H_{\text{ex}z} \equiv (\mathbf{H}_{\text{ex}} \cdot \hat{z})_{\Omega=\pi/2} = -\frac{2A}{M_s \delta^2} \cos \phi. \quad (\text{A4})$$

It is worth noticing that if the metric factors h_{η} and h_{μ} are η independent, $\partial h_{\eta}/\partial \eta = \partial h_{\mu}/\partial \eta = 0$, and then $H_{\text{ex}\eta} = 0$. Therefore, we can state that the tangential exchange field is directly associated with the metric variations along the length of the NW. In other words, $H_{\text{ex}\eta}$ is induced by the curvature gradient along the η direction. Furthermore, we note that $h \equiv h_{\eta} = h_{\mu}$ (which occurs in the case of the elliptically bent NW, as well as in the case of the parabolic and hyperbolic geometries), the tangential component of the exchange-driven curvature-induced effective field becomes independent of the DW phase ϕ , that is,

$$H_{\text{ex}\eta} = -\frac{2A}{M_s \delta h^2} \frac{\partial h}{\partial \eta}. \quad (\text{A5})$$

We highlight that our results also apply to a tail-to-tail DW by performing the change $\delta \rightarrow -\delta$.

- [1] V. V. Slastikov and C. Sonnenberg, *IMA J. Appl. Math.* **77**, 220 (2012).
 [2] R. Wieser, E. Y. Vedmedenko, P. Weinberger, and R. Wiesendanger, *Phys. Rev. B* **82**, 144430 (2010).
 [3] A. Wattle, B. Trapp, M. Staño, C. Thirion, S. Bochmann, J. Bachmann, M. Foerster, L. Aballe, T. O. Mentès, A. Locatelli,

- A. Sala, L. Cagnon, J.-C. Toussaint, and O. Fruchart, *Phys. Rev. B* **99**, 024433 (2019).
 [4] M. Schöbitz, A. De Riz, S. Martin, S. Bochmann, C. Thirion, J. Vogel, M. Foerster, L. Aballe, T. O. Mentès, A. Locatelli, F. Genuzio, S. Le-Denmat, L. Cagnon, J.-C. Toussaint, D. Gusakova, J. Bachmann, and O. Fruchart, *Phys. Rev. Lett.* **123**, 217201 (2019).

- [5] S. Parkin and S. H. Yang, *Nat. Nanotechnol.* **10**, 195 (2015).
- [6] C. I. L. de Araujo, J. C. S. Gomes, D. Toscano, E. L. M. Paixão, P. Z. Coura, F. Sato, D. V. P. Massote, and S. A. Leonel, *Appl. Phys. Lett.* **114**, 212403 (2019).
- [7] S. Sharma, B. Muralidharan, and A. Tulapurkar, *Sci. Rep.* **5**, 14647 (2015).
- [8] O. O. Toro, S. G. Alves, V. L. Carvalho-Santos, and C. I. L. de Araujo, *J. Appl. Phys.* **127**, 183905 (2020).
- [9] D. E. Nikonov, S. Manipatruni, and I. A. Young, *J. Appl. Phys.* **115**, 213902 (2014).
- [10] D. A. Allwood, G. Xiong, C. C. Faulkner, D. Atkinson, D. Petit, and R. P. Cowburn, *Science* **309**, 1688 (2005).
- [11] H. Cui, L. Cai, X. Yang, S. Wang, M. Zhang, C. Li, and C. Feng, *Appl. Phys. Lett.* **112**, 092404 (2018).
- [12] A. P. Espejo, F. Tejo, N. Vidal-Silva, and J. Escrig, *Sci. Rep.* **7**, 4736 (2017).
- [13] N. L. Schryer and L. R. Walker, *J. Appl. Phys.* **45**, 5406 (1974).
- [14] A. Mougin, M. Cormier, J. P. Adam, P. J. Metaxas, and J. Ferré, *Europhys. Lett.* **78**, 57007 (2007).
- [15] M. Yan, Á. Kákay, S. Gliga, and R. Hertel, *Phys. Rev. Lett.* **104**, 057201 (2010).
- [16] D. Altbir, J. M. Fonseca, O. Chubykalo-Fesenko, R. M. Corona, R. Moreno, V. L. Carvalho-Santos, and Y. P. Ivanov, *Sci. Rep.* **10**, 21911 (2020).
- [17] R. Moreno, V. L. Carvalho-Santos, A. P. Espejo, D. Laroze, O. Chubykalo-Fesenko, and D. Altbir, *Phys. Rev. B* **96**, 184401 (2017).
- [18] R. Cacilhas, C. I. L. de Araujo, V. L. Carvalho-Santos, R. Moreno, O. Chubykalo-Fesenko, and D. Altbir, *Phys. Rev. B* **101**, 184418 (2020).
- [19] K. V. Yershov, V. P. Kravchuk, D. D. Sheka, and Y. Gaididei, *Phys. Rev. B* **93**, 094418 (2016).
- [20] G. H. R. Bittencourt, R. Moreno, R. Cacilhas, O. Chubykalo-Fesenko, D. Altbir, and V. L. Carvalho-Santos, *Appl. Phys. Lett.* **118**, 142405 (2021).
- [21] V. L. Carvalho-Santos, M. A. Castro, D. Salazar-Aravena, D. Laroze, R. M. Corona, S. Allende, and D. Altbir, *Appl. Phys. Lett.* **118**, 172407 (2021).
- [22] Y. Gaididei, V. P. Kravchuk, and D. D. Sheka, *Phys. Rev. Lett.* **112**, 257203 (2014).
- [23] O. M. Volkov, A. Kákay, F. Kronast, I. Mönch, M.-A. Mawass, J. Fassbender, and D. Makarov, *Phys. Rev. Lett.* **123**, 077201 (2019).
- [24] A. Korniienko, A. Kákay, D. D. Sheka, and V. P. Kravchuk, *Phys. Rev. B* **102**, 014432 (2020).
- [25] V. P. Kravchuk, D. D. Sheka, A. Kákay, O. M. Volkov, U. K. Röβler, J. van den Brink, D. Makarov, and Y. Gaididei, *Phys. Rev. Lett.* **120**, 067201 (2018).
- [26] K. V. Yershov, V. P. Kravchuk, D. D. Sheka, O. V. Pylypovskiy, D. Makarov, and Y. Gaididei, *Phys. Rev. B* **98**, 060409(R) (2018).
- [27] K. V. Yershov, V. P. Kravchuk, D. D. Sheka, and Y. Gaididei, *Phys. Rev. B* **92**, 104412 (2015).
- [28] R. Moreno, V. L. Carvalho-Santos, D. Altbir, and O. Chubykalo-Fesenko, *J. Magn. Magn. Mater.* **542**, 168495 (2022).
- [29] M. Charilaou, H.-B. Braun, and J. F. Löffler, *Phys. Rev. Lett.* **121**, 097202 (2018).
- [30] A. Thiaville, Y. Nakatani, J. Miltat, and Y. Suzuki, *Europhys. Lett.* **69**, 990 (2005).
- [31] A. Aharoni, *J. Appl. Phys.* **83**, 3432 (1998).
- [32] E. Saitoh, H. Miyajima, T. Yamaoka, and G. Tatara, *Nature* **432**, 203 (2004).
- [33] W. Döring, *Z. Naturforsch.* **3**, 373 (1948).
- [34] A. Thiaville and Y. Nakatani, Domain-wall dynamics in nanowires and nanostrips, in *Topics in Applied Physics: Spin Dynamics in Confined Magnetic Structures III*, edited by B. Hillebrands and A. Thiaville (Springer-Verlag, Heidelberg, 2006).
- [35] S. Zhang and Z. Li, *Phys. Rev. Lett.* **93**, 127204 (2004).
- [36] V. Raposo, S. Moretti, M. A. Hernandez, and E. Martinez, *Appl. Phys. Lett.* **108**, 042405 (2016).
- [37] J. Mejía-López, E. A. Velásquez, J. Mazo-Zuluaga, and D. Altbir, *Nanotechnology* **29**, 345702 (2018).
- [38] M. Xu, R. Li, J. Zhang, and D. Meng, *Solid State Commun.* **329**, 114259 (2021).
- [39] L. Fan, J. Hu, Y. Su, and J. Zhu, *J. Magn. Magn. Mater.* **401**, 484 (2016).